Available online at www.sciencedirect.com

ScienceDirect

www.journals.elsevier.com/jes

JES JOURNAL OF ENVIRONMENTAL SCIENCES

www.jesc.ac.cn

Assessing the effects of surface-bound humic acid on the phototoxicity of anatase and rutile TiO_2 nanoparticles *in vitro*

Xiaojia He[1], *Sabrieon Sanders*[2], *Winfred G. Aker*[3], *Yunfeng Lin*[4], *Jessica Douglas*[5], *Huey-min Hwang*[1,*]

1. *Department of Biology, Jackson State University, Jackson, MS, USA*
2. *Department of Biological Sciences, Alcorn State University, Lorman, MS, USA*
3. *Environmental Science Ph.D. Program, Jackson State University, Jackson, MS, USA*
4. *Department of Chemistry and Biochemistry, Jackson State University, Jackson, MS, USA*
5. *School of Polymers and High Performance Materials, The University of Southern Mississippi, Hattiesburg, MS, USA*

ARTICLE INFO

Article history:
Received 18 March 2015
Revised 17 May 2015
Accepted 22 May 2015
Available online 1 September 2015

Keywords:
TiO_2 nanoparticles
Escherichia coli
Humic acid
Crystallinity
Surface coating

ABSTRACT

In this study, the cytotoxicity of two different crystal phases of TiO_2 nanoparticles, with surface modification by humic acid (HA), to *Escherichia coli*, was assessed. The physicochemical properties of TiO_2 nanoparticles were thoroughly characterized. Three different initial concentrations, namely 50, 100, and 200 ppm, of HA were used for synthesis of HA coated TiO_2 nanoparticles (denoted as A/RHA50, A/RHA100, and A/RHA200, respectively). Results indicate that rutile (LC_{50} (concentration that causes 50% mortality compared the control group) = 6.5) was more toxic than anatase (LC_{50} = 278.8) under simulated sunlight (SSL) irradiation, possibly due to an extremely narrow band gap. It is noted that HA coating increased the toxicity of anatase, but decreased that of rutile. Additionally, AHA50 and RHA50 had the biggest differences compared to uncoated anatase and rutile with LC_{50} of 201.9 and 21.6, respectively. We then investigated the formation of reactive oxygen species (ROS) by TiO_2 nanoparticles in terms of hydroxyl radicals ($^{\cdot}OH$) and superoxide anions ($O_2^{\cdot-}$). Data suggested that $O_2^{\cdot-}$ was the main ROS that accounted for the higher toxicity of rutile upon SSL irradiation. We also observed that HA coating decreased the generation of $^{\cdot}OH$ and $O_2^{\cdot-}$ on rutile, but increased $O_2^{\cdot-}$ formation on anatase. Results from TEM analysis also indicated that HA coated rutile tended to be attached to the surface of *E. coli* more than anatase.

Introduction

Titanium dioxide (TiO_2) nanoparticles are the most widely used photocatalyst for environmental remediation (Chen and Mao, 2007; Kwon et al., 2008), particularly in natural aquatic environments. However, recent studies have raised the concerns over the potential health risks to humans and environments caused by nano TiO_2 throughout its life cycle (Boxall et al., 2007; Sharma, 2009; He et al., 2014b). The behavior and fate of TiO_2 nanoparticles can be altered by suspended solids and dissolved organic matter (DOM), once they are released into aquatic environments. In addition, the lack of knowledge of nano-bio-eco interactions could limit the use of TiO_2 nanoparticles for field applications. Therefore, it is imperative that their

* *Corresponding author*. E-mail: hwang@jsums.edu (Huey-min Hwang).

http://dx.doi.org/10.1016/j.jes.2015.05.028
1001-0742/

physicochemical properties be assessed by conducting feasibility studies before we employ such nanotechnology for environmental remediation.

In general, unmodified TiO_2 nanoparticles can only be excited by UV light, owing to their large band gap (theoretically 3.0 eV for rutile and 3.2 eV for anatase). However, TiO_2 nanoparticles can be sensitized through specific photosensitizers, for instance, dyes (Persson et al., 2000; De Angelis et al., 2007). Recently, humic acid (HA) has also been suggested to be capable of serving as a photosensitizer in HA/TiO_2/visible light system (Selli et al., 1999; Cho and Choi, 2002; Ryu and Choi, 2004). The supplementation with HA essentially expands the applicability of TiO_2 as a photocatalyst into visible light region. In addition, TiO_2 nanoparticles on most occasions, tend to aggregate in aqueous solutions and exist as aggregates, normally over 1 μm. Appreciably, surface coating can largely improve the stability and dispersibility of TiO_2 nanoparticles in aqueous solutions. Thus, lately, the physicochemical properties of HA coated TiO_2 nanoparticles have been studied and reported (Yang and Xing, 2009; Chen et al., 2012). Besides the expanded spectrum of light excitation, HA coated TiO_2 nanoparticles may also differ from the uncoated TiO_2 nanoparticles in the presence of free HA (Lin et al., 2012). It was reported that HA coating could reduce the adhesion of TiO_2 nanoparticles to algal cells, decrease the formation of reactive oxygen species (ROS), and consequently alleviate the algal toxicity (Lin et al., 2012). However, Yang et al. (2013) reported that oxidative deoxyribonucleic acid (DNA) damage and toxicity to zebrafish (*Danio rerio*) were increased by the supplement of HA to TiO_2 nanoparticles in the absence of light irradiation (Yang et al., 2013). Thus, it is necessary to investigate the alteration of physicochemical properties of TiO_2 nanoparticles coated with HA and to assess the effects on the subsequent nanotoxicity in the presence of sunlight or only visible light.

Furthermore, the effect of crystallinity has also been suggested to be attributed to the different toxicological profiles of TiO_2 nanoparticles. It is generally recognized that anatase is more active and toxic than rutile under UV irradiation. According to Luttrell et al. (2014), this is owing to the larger band gap of anatase. Under UV irradiation, anatase TiO_2 nanoparticles could generate higher amounts of ROS intracellularly and extracellularly than the rutile phase (Chen et al., 2007; Guichard et al., 2012). However, this could be altered or even reversed under visible light irradiation, or in the absence of light, as substantiated by the reports (Sayes et al., 2006; Lipovsky et al., 2012; Numano et al., 2014). Notably, ROS formation in water suspensions of TiO_2 was much higher in rutile than anatase after visible light illumination (400–800 nm, 40 mW/cm^2) (Lipovsky et al., 2012). They suggested that the difference between anatase and rutile under visible illumination might be owing to a difference in their band-gap energies (E_g), in which E_g (anatase) = 3.2 eV (387 nm), and E_g (rutile) = 3 eV (415 nm). On the basis of the above consideration, it is important to investigate how the photoactivity and toxicity differ with crystallinity under sunlight irradiation.

In this study, we synthesized HA coated TiO_2 nanoparticles in both rutile and anatase phases. We investigated their toxicity to *Escherichia coli* (*E. coli*) under simulated sunlight (SSL) irradiation. To the best of our knowledge, no study has been reported to have specifically investigated the effect of surface-bound HA on the physicochemical properties and toxicity of TiO_2 nanoparticles to living organisms.

1. Materials and methods

1.1. Materials

TiO_2 nanoparticles (Sample A and Sample B) were purchased from US Research Nanomaterials, Inc. (US Research Nanomaterials, Inc., Houston, TX, USA). All organic solvents and the humic acid (>99%) used in this study were purchased from Sigma Aldrich (Sigma-Aldrich Co., St. Louis, MO, USA). All solutions were prepared using nanopure water (Thermo Scientific™ NERL™ Reagent Grade Water, Nerl Diagnostics LLC, East Providence, RI, USA). Bacteria *E. coli* (ATCC#25254) was purchased from the American Type Culture Collection (ATCC, Manassas, VA, USA).

1.2. Preparation of HA coated TiO_2

The steps of synthesis of HA coated TiO_2 followed the previous description of (Yang and Xing, 2009) with slight modifications. Briefly, 1 g of TiO_2 (Sample A or Sample B) was added into 100 mL of HA solution to reach the different final concentrations of 50, 100, and 200 ppm. After stirring for 2 day at 180 r/min, the mixture was then centrifuged at 5000 ×*g* for 30 min and washed three times with nanopure water to eliminate any unbounded HA residues. The pellet was collected after removing the supernatant, and freeze-dried. Lyophilization was then conducted under vacuum at 0.014 mbar for 48 hr with a Labconco Freezone Plus 2.5 L Benchtop Cascade Freeze Dry Systems (Labconco, USA) equipped with a Welch 8912Z-02 Vacuum (Welch 8912Z-02, Gardner Denver Welch Vacuum Technology Inc., USA). Samples A and B were identified by X-ray diffraction (XRD) as anatase TiO_2, and rutile TiO_2, respectively. AHA50, AHA100, and AHA200 were the products from 50, 100, and 200 ppm HA coated with Sample A (anatase TiO_2) respectively. Correspondingly, RHA50, RHA100, and RHA200 were 50, 100, and 200 ppm HA coated with Sample B (rutile TiO_2), respectively.

1.3. Characterization

The characterization of HA coated TiO_2 nanoparticles was conducted with XRD, transmission electron microscopy (TEM), scanning electron microscopy (SEM), energy dispersive X-ray spectroscopy (EDX), Fourier transform infrared spectroscopy (FTIR), UV-Vis spectroscopy, dynamic light scattering (DLS), and phase analysis light scattering (PALS). The content of coated HA was determined with total organic carbon (TOC) analysis.

XRD patterns were obtained using a Rigaku D/MAX-Ultima-III diffractometer (Rigaku D/MAX-Ultima-III diffractometer, Rigaku, Japan) at room temperature with Cu Kα radiation at a tube current of 44 mA and an acceleration voltage of 40 kV. The scan ranges were 2–40° and 2–75° at a step interval of 0.1° and a scanning rate of 0.05°/min. Primary nanoparticle size was determined using a Jeol, JEM 1011 electron microscope working at 100 kV (JEM 1011, Joel USA, Inc., USA) equipped with a Gatan camera model 785. Morphology of TiO_2 and variation of growth for synthesized HA coated TiO_2 were

also studied using a SEM (SIGMA VP, Carl Zeiss, Germany) operating at 10 kV at a working distance of 3.3–3.7 mm. The elemental composition of the nanocomposite was studied using EDX with a Thermo Scientific Ultra Dry EDS Detector (Thermo Scientific, USA) operating at 20 kV.

Uncoated TiO_2 and the HA-coated variants were also characterized by FT-IR using a Nexus 870 FTIR spectrometer (Nexus 870, Thermo-Nicolet, USA). Absorbance spectra of the tested TiO_2 were measured using a UV–Vis spectrophotometer (UV-2600, Shimadzu, Japan). The hydrodynamic size and zeta potential values of suspensions of the tested TiO_2 at 100 ppm in nanopure water were obtained *via* DLS and PALS, respectively, using a Malvern Zetasizer Nano (Malvern Instruments Ltd, UK). Nanoparticle suspension was sonicated (FS30, Fisher Scientific, USA) in water for 30 min and kept in dark until use. The stock solution was sonicated for 10 min prior to experimentation. The pH adjustment of PALS was achieved by the addition of 0.025 mol/L HCl or 0.025 mol/L NaOH solution.

TOC was analyzed using an Elementar Combustion Instrument (Vario Macro CNS, Elementar, Germany). Approximately a 70 to 80 mg sample was dropped into a combustion chamber where it was consumed at 1150°C; the post-combustion temperature was 800°C, and the reduction tube was at 850°C. Once combustion took place, the gases were swept sequentially to a thermoconductivity (TC) detector by Helium gas at 499 mL/min. Nitrogen was measured immediately while the carbon and sulfur gases were adsorbed onto their respective columns and released to the TC detector, carbon first, and then sulfur. Initial combustion was carried out with an injection of oxygen, first at stage 1 for 30 sec at 30 mL/min, and then at stage 2 for 120 sec at 100 mL/min.

1.4. Cytotoxicity test

The TiO_2 stock solutions (1000 ppm) used in this study include anatase, AHA50 and AHA200, rutile, RHA50 and RHA200. The stock solutions were autoclaved to eliminate any contaminant microorganisms, allowed to cool to room temperature, then used immediately for the cytotoxicity tests. The effect of autoclaving on the physicochemical properties and toxicity of TiO_2 was also evaluated. No significant difference was observed with regard to the effect of autoclaving (data not shown). All stock solutions were sonicated (FS30, Fisher Scientific, USA) for 30 min prior to adding them to make the working solution. It was reported that sonication of nanoparticles has a minimal effect on particle surface charge. Sonication has been utilized to facilitate particle dispersion and solution mixture (Warheit, 2008).

Cytotoxicity testing was performed by inoculating bacterial cells on Miller Luria-Bertani Broth (LB) agar plates after treatment with TiO_2 solutions of various concentrations. An inoculation loop of *E. coli* suspension was introduced into LB nutrient broth and cultured overnight at 37°C. Following incubation, the culture was washed three times with sterilized physiological saline (0.8% W/V) in a centrifuge (Eppendorf Centrifuge 5810 R, Eppendorf AG, Germany) at 4°C and 1735 ×*g* for 10 min. The bacterial suspensions were diluted (10^6 × dilution factor) and exposed to the TiO_2 in quartz test tubes (ACE Glass Inc., Louisville, USA). Subsequently, they were then exposed to simulated sunlight for 1 hr with stirring. A PMA 2100 radiometer (PMA 2100, Solar Light Co., USA) equipped with UVA probe PMA 2110 and visible light probe PMA 2130 (PMA 2130, Solar Light Co., USA) was used to measure the light intensity during exposure (visible light: average 22.95 ± 0.16 W/m^2, total in 1 hr 83.70 kJ/m^2; UVA: average 0.18 ± 0.00 mW/cm^2, total in 1 hr 0.70 J/cm^2). Dark exposure was also conducted in quartz tubes and wrapped in aluminum foil to prevent light illumination.

After exposure, 100 μL aliquots of the samples were spread on respective LB agar and then placed in an incubator at 37°C for 24 hr. LC_{50} (concentration that causes 50% mortality compared to the control group) was then calculated (Cook et al., 2010).

1.5. Assessment of ROS formation

1.5.1. Hydroxyl radicals (·OH)

Hydroxyl radical (·OH) generation by TiO_2 nanoparticles was quantified by fluorescence spectroscopy using terephthalic acid (Ishibashi et al., 2000; Yu et al., 2009). Owing to its high sensitivity and reliability, terephthalic acid is able to specifically react with ·OH, producing fluorescent 2-hydroxyterephthalic acid. Briefly, TiO_2 solution was added into 5 mL of 5×10^{-4} mol/L terephthalic acid with NaOH at 2×10^{-3} mol/L. The mixture was then stirred in the dark for 2 hr to reach equilibrium. After that, the solution was immediately exposed to simulated sunlight irradiation for 1 hr. Prior to fluorescence spectroscopy, the reaction mixture was filtered through a membrane filter (pore size 0.22 μm, diameter 13 mm, polyvinylidene fluoride (PVDF), Fisher Sci., USA). Fluorescence intensity was measured at 425 nm (scanned from 350 to 600 nm with 1 nm slit) excited by 315 nm light with a Horiba Scientific Fluoromax-4 spectrofluorometer (Horiba Jobin Yvon Inc., USA) equipped with a NanoLED pulsed diode light source.

1.5.2. Superoxide ($O_2^{\cdot-}$)

The formation of superoxide ($O_2^{\cdot-}$) was detected by using a nitro blue tetrazolium (NBT) assay. Superoxide ions can reduce NBT to insoluble purple formazan (Goto et al., 2004). Briefly, TiO_2 samples of various concentrations were added into 5 mL solutions of 0.1 mmol/L NBT in quartz test tubes. The respective mixtures were then stirred thoroughly and exposed to simulated sunlight for 1 hr under stirring. Subsequently, 0.22 μm PVDF membrane filters were used to filter out precipitates prior to UV–Vis spectroscopy. The generation of $O_2^{\cdot-}$ was quantified by measuring the reduction of NBT at 260 nm. The final solutions containing NBT were diluted twofold in order to reach an optimal optical reading. Accordingly, results were multiplied by two for quantitation.

1.6. TEM analysis of nano-bio interactions

Bacterial suspension was prepared for TEM measurements. For observing attachment of nanoparticles, a 20 μL aliquot of treated bacterial suspension was spread onto a TEM copper grid (CF300-Cu, Electron Microscopy Sciences, USA). After drying out at ambient temperature, TEM micrographs were captured and analyzed using a Jeol, JEM 1011 electron microscope working at 100 kV (JEM 1011, Joel USA, Inc., USA) equipped with a Gatan camera model 785.

1.7. Statistical analysis

Data in triplicate were presented as mean ± standard deviation (SD). The data were subjected to statistical analysis by one-way analysis of variance (ANOVA) followed by Tukey's method for multiple comparisons. Values of $p < 0.05$ and $p < 0.01$ were considered significant and extremely significant, respectively. The statistical analyses were performed using SAS 9.2 statistical program (SAS Institute, Cary, NC, USA).

2. Results and discussion

2.1. Physicochemical properties of TiO_2 nanoparticles

The X-ray diffraction pattern of the TiO_2 nanoparticles used in this study is shown in Fig. 1 and the peak details are in Table S1. Our experimental XRD pattern agrees with the JCPDS 71-1166 (anatase TiO_2) and JCPDS 72-1148 (rutile TiO_2), and the XRD pattern of TiO_2 nanoparticles reported in other literature (Kavei et al., 2011). 2θ at peak 25.2 and 27.5° confirms the TiO_2 anatase and rutile structures, respectively. It is noted that the XRD patterns in Fig. 1 indicate that both Samples A and B were crystalline and broad diffraction peaks suggesting small sized crystallite. XRD patterns suggested that Sample A and Sample B were 100% anatase and 100% rutile TiO_2, as shown in Fig. 1a and b, respectively.

The UV–Vis absorption spectra of the tested nanoparticles are shown in Fig. 2a and b. It is seen that the HA coating on rutile TiO_2 resulted in a reduction in photo-absorption. However, the HA coating on anatase increased the light absorbance of TiO_2. The band-gap energies of the TiO_2 variants can be estimated from the plots of the photon energy and the results are shown in Fig. 2c and d. The band-gap energy (E_g) of the un-coated TiO_2 is estimated to be 3.5 and 2.31 eV, for anatase and rutile TiO_2, respectively. The band gap of anatase was

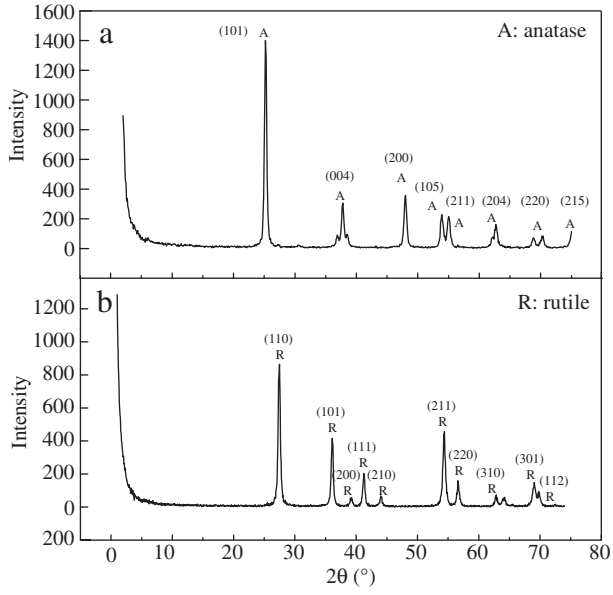

Fig. 1 – XRD (X-ray diffraction) patterns of (a) Sample A and (b) Sample B TiO_2 used in this study.

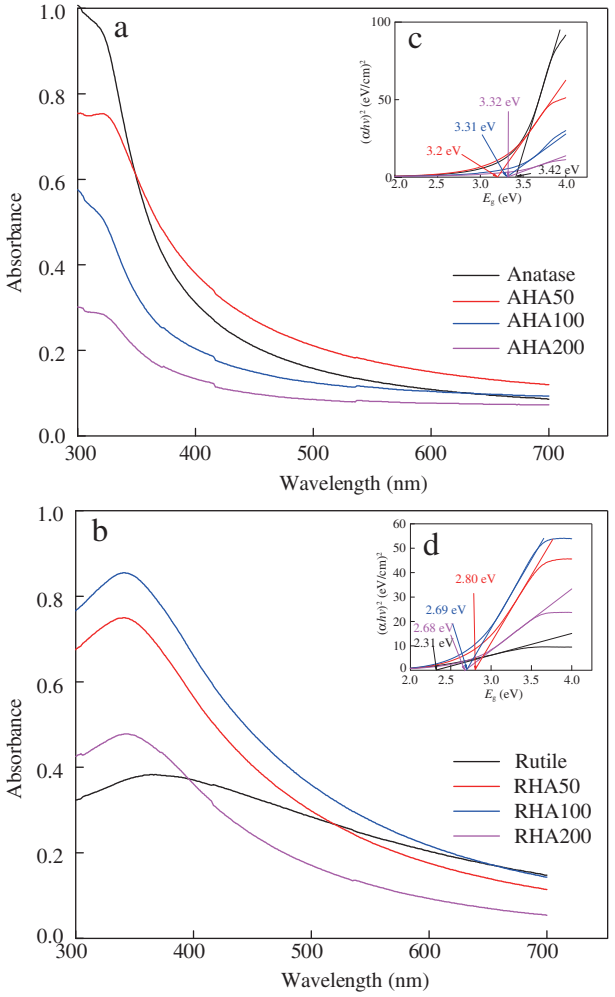

Fig. 2 – Light absorbance and band gap of (a) anatase TiO_2 nanoparticles with and without humic acid (HA) coating and (b) rutile TiO_2 nanoparticles with and without HA coating. (c) and (d) were the plots of $(\alpha h\nu)^2$ *versus* $(h\nu)$ for (a) and (b), respectively. AHA50, AHA100, and AHA200 were the products from 50, 100, and 200 ppm HA coated with Sample A (anatase TiO_2), and RHA50, RHA100, and RHA200 were 50, 100, and 200 ppm HA coated with Sample B (rutile TiO_2), respectively.

higher compared with the theoretical band gap of anatase (3.2 eV), while it was lower for rutile compared with the theoretical band gap of rutile (3.0 eV). The HA coated anatase TiO_2 revealed new deep levels which are located at 3.2, 3.31, and 3.32 eV, for AHA50, AHA100, and AHA200, respectively. For rutile TiO_2, however, the HA coating resulted in an increase in the band gap to 2.68, 2.69, and 2.80 eV, for RHA200, RHA100, and RHA50, respectively. Intriguingly, it seems that the HA coating altered the band gap property of the TiO_2 nanoparticles. However, this change was attributed to photosensitization of HA on the surface of TiO_2, which will be illustrated in the next section.

Based on the measured TOC contents in the TiO_2/HA, it was calculated that AHA50, AHA100, and AHA200 contained 0.5% (W/W), 0.8% (W/W), and 0.8% (W/W) of HA in terms of carbon content, respectively. For HA coated rutile TiO_2, the HA

content was 0.4% (W/W), 0.8% (W/W), and 0.7% (W/W) for RHA50, RHA100, and RHA200, respectively. The linear increase of the coating percentage from HA50 to HA100 implied that HA coating on TiO_2 proceeded with multilayer formation. In contrast, the data indicated that there was no significant difference between the HA coated TiO_2 prepared at 100 and 200 ppm, in terms of coating percentage. This fact is in agreement with the band gap results. Thus, we chose 200 ppm HA coated TiO_2 for further analysis and testing. It is noteworthy that there is no significant difference among surface coating in terms of sulfur and nitrogen (data not shown).

Furthermore, the primary size of TiO_2 was revealed using TEM, as shown in Fig. 3a–f and Table 1. The TEM images show that the tested rutile and anatase TiO_2 nanoparticles were in the same size range. We also found that humic acid, as a surface coating, had no significant effect on the primary size of anatase or rutile TiO_2 nanoparticles. The two-dimensional (2-D) surface morphological study of the HA loaded TiO_2 nanoparticles was carried out by SEM (Fig. 3g–j). The morphology and structure of the samples were further investigated by EDX spectroscopy. The elemental compositions are thus further confirmed. EDX point spectra taken from the center point of TiO_2 show strong Ti and O signals (Fig. 3k–n). As shown in Fig. 3l and n, N signals were also observed for HA coated TiO_2. The chemical compositions of the thin films analyzed are given in Fig. S1–8.

The FTIR spectra of the tested TiO_2 with and without HA coating are presented in Fig. 4. The data indicate that the observed peak of rutile TiO_2 at 1639 cm^{-1} shifted to 1629, 1627, and 1631 cm^{-1} for RHA50, RHA100, and RHA200, respectively. As shown in Fig. 4a, absorption spectra suggest strong interactions of phenolic OH of HA with TiO_2. Interestingly, RHA100 exhibited the largest shift as well as the strongest absorbance. This may be due to ligand exchange between TiO_2 and HA and a larger band gap of RHA100 (Fig. 2b). A similar shift was also observed for anatase TiO_2 around 1600–1700 cm^{-1}, as shown in Fig. 4b. In comparison with pure anatase TiO_2, several continuous new peaks around 1300–1500 cm^{-1} appeared after binding with HA, owing to the C = C and C = O stretch of HA, particularly, the tiny peak around 1300, 1372 and 1537 cm^{-1} should be v_s(C–O), v_{as}(COO–), and v_s(COO–). In addition, the peak of OH stretching at 3300–3600 cm^{-1} may come from a different extent of ligand exchange between phenolic groups in TiO_2 and HA. We also found that as the amount of HA increased, the peak at 2350–2400 became weaker, owing to the strong interactions of phenolic OH with TiO_2. Compared with the ones coated with HA at 100 and 50 ppm, there is a sharp increase in the intensity of the peak of the hydroxyl group, around 3500 cm^{-1}, in rutile TiO_2 after coating with HA at 200 ppm. This could occur as a result of the ligand exchange between hydroxyl groups on TiO_2 and HA carboxyl/hydroxyl functional groups (Yang and Xing, 2009). From this observation, HA chemically bound on the surface of TiO_2 nanoparticles.

In addition, hydrodynamic size and zeta potential were investigated as aspects of chemical characterization. Because of their lipophilicity, the rutile TiO_2 nanoparticles form larger

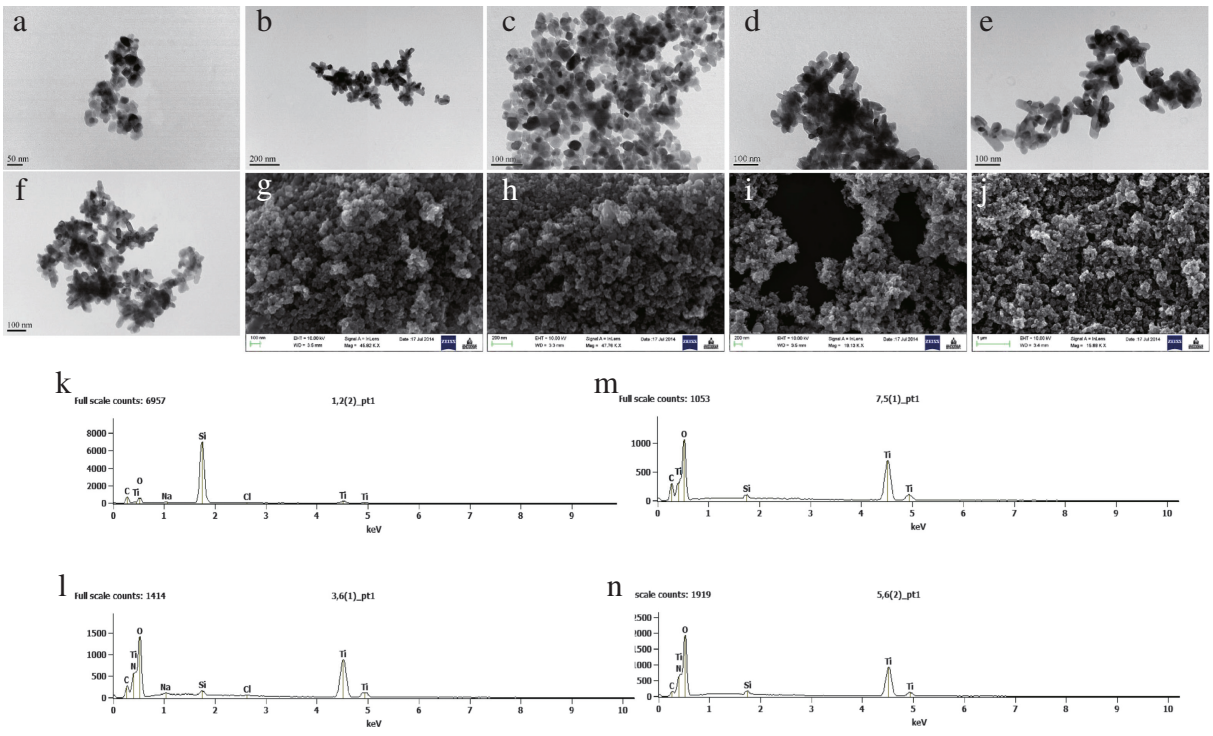

Fig. 3 – TEM micrographs of (a) anatase, (b) AHA50, (c) AHA200, (d) rutile, (e) RHA50, (f) RHA200, FESEM images of (g) anatase, (h) AHA200, (i) rutile, (j) RHA200, EDX point spectra and line scans of (k) anatase, (l) AHA200, (m) rutile, and (n) RHA200. Si peaks are attributed to the silicon wafers for imaging. Other elements such as Na and Cl are the components of substrate. TEM: transmission electron microscopy; EDX: energy dispersive X-ray spectroscopy; FESEM: field emission SEM; SEM: scanning electron microscopy.

Table 1 – Characterization of TiO_2 with and without humic acid (HA) coating.

Nanoparticles	Anatase	AHA50	AHA200	Rutile	RHA50	RHA200
Primary size (nm)	25.1 ± 5.7	31.4 ± 5.4	22.9 ± 8.3	34.5 ± 4.5	28.1 ± 5.3	30.6 ± 4.5
Primary size distribution (nm)	11.5–32.5	25.5–42	13.5–41	28–42	20.5–33	24–35.5
Hydrodynamic size (z-average, nm)	1285.0	554.6	526.1	2228.1	635.7	634.4
Hydrodynamic size distribution (nm)	220–1484	68–825	79–459	531–1990	79–718	79–615
Zeta potential (mV) at pH 7.0	−22.8	−24	−25	−24.5	−28	−25
Isoelectric point (IEP)	3.9	4.6	4.9	4.1	4.3	5.7

AHA50 and AHA200 were the products from 50 and 200 ppm HA coated with Sample A (anatase TiO_2), and RHA50 and RHA200 were 50 and 200 ppm HA coated with Sample B (rutile TiO_2), respectively.

aggregates in aqueous media. As shown in Fig. 4c, the coating of HA greatly reduced the size distribution of TiO_2 in aqueous solutions. It is notable that the average size was also reduced (Table 1). Correspondingly, the absolute value of the zeta potential increased at the same pH value after HA coating (Fig. 4d). Moreover, HA coating induced a shift in isoelectric point (IEP) to pH values substantially higher than its pristine IEP.

2.2. Cytotoxicity of TiO_2 to *E. coli*

Based on the results of viability testing with *E. coli* (Fig. 5) and the computed LC_{50} values (Table 2), it is apparent that rutile TiO_2 was more toxic than anatase TiO_2. The higher toxicity may be due to the lower band-gap energy of rutile TiO_2 and consequent better light absorbance in visible light compared to that of anatase TiO_2 (Fig. 2). The change in light absorption is consistent with cytotoxicity test results, while being bi-directional in this property with the increase in HA coating degree. It is widely reported that anatase is more toxic than rutile in the presence of UV light irradiation, while it is less toxic than rutile in the absence of light (Numano et al., 2014). Owing to the larger band gap of anatase in comparison to rutile, it tends to be more active under UV light (Kakinoki et al., 2004; Tayade et al., 2007). In this study, neither anatase nor rutile exhibited toxicity to *E. coli* in the dark (data not shown). However, the toxicity dramatically increased under SSL exposure, particularly in the case of rutile. It seems that our results

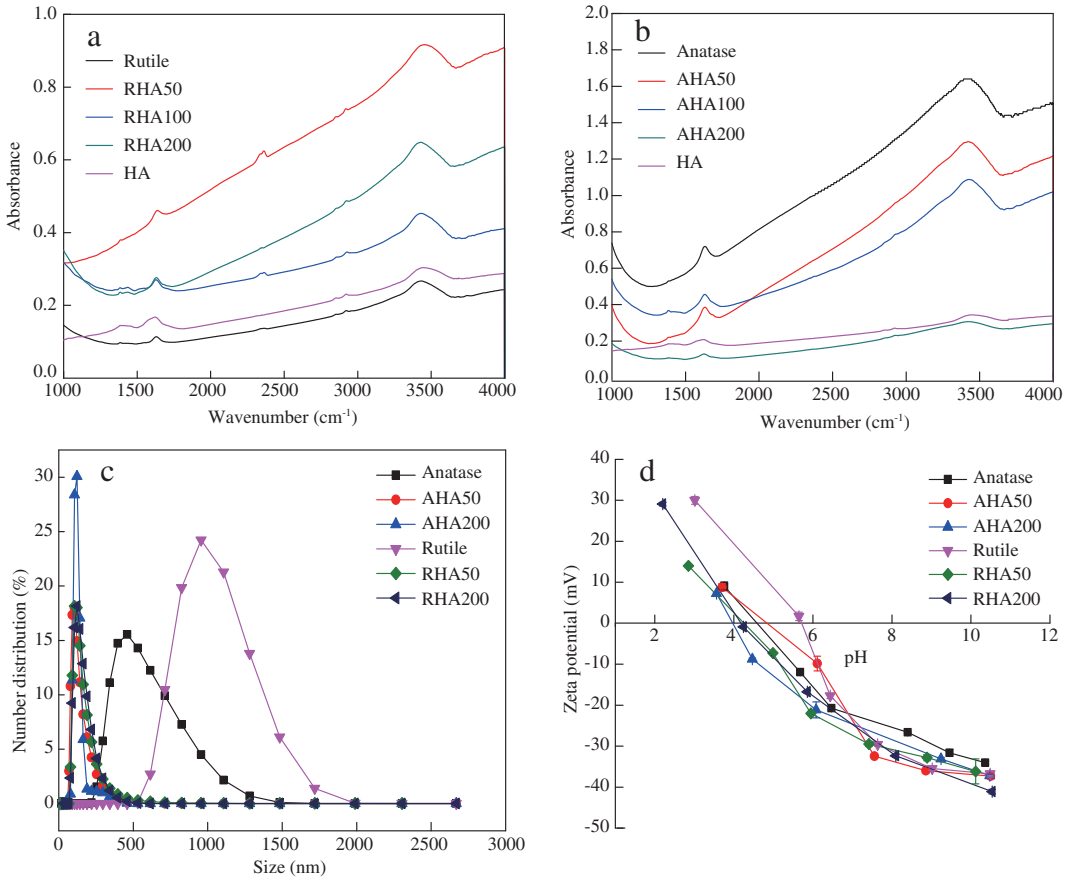

Fig. 4 – FTIR for (a) rutile and (b) anatase TiO_2 with and without HA coating, and (c) hydrodynamic size distribution and (d) zeta potential of TiO_2. FTIR: Fourier transform infrared spectroscopy; HA: humic acid.

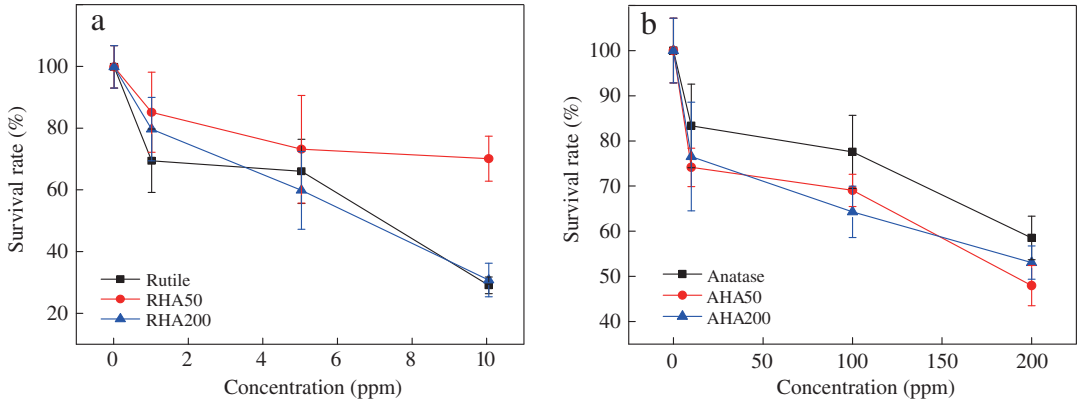

Fig. 5 – Viability of *Escherichia coli* (*E. coli*) after exposure to (a) anatase and (b) rutile TiO_2 under simulated sunlight.

disagree with some published data (Sayes et al., 2006; Braydich-Stolle et al., 2009). However, differences in the light conditions used in the aforementioned studies account for the variances, owing to the extremely low band gap of rutile used in this study. It should be noted that the aggregation state of TiO_2 nanoparticles may alter their ultimate bioavailability. In the present study, there was no notable difference in the extent of aggregation among the HA coated TiO_2. Hence, the big difference between uncoated anatase and rutile did not contribute to their distinct performance in causing toxicity to *E. coli*, indicating that the bioavailability may not be the major factor for causing higher toxicity by rutile.

In addition to crystallinity, our statistical analysis indicates that surface coating with HA exhibited significant impact on the phototoxicity of TiO_2 ($p < 0.05$, Table 3). It is apparent that surface coating of HA increased the toxicity of anatase, but decreased the toxicity of rutile. Additionally, the alteration of toxicity was related to the percentage of HA coating. The results suggested that AHA50 and RHA50 had the biggest differences compared to uncoated anatase and rutile, respectively. The LC_{50} values of AHA50 and RHA50 decreased by 27.6% and 332%, respectively. This pattern is consistent with band gap properties in Fig. 2. The lower coating percentage of HA tended to increase the band gap of rutile more intensively, leading to a subsequent narrowing of the light absorption band and decreased phototoxicity. However, the lower coating percentage of HA was more capable of lowering bang gap of anatase, resulting in expanded light absorption and increased phototoxicity. This change suggests that there is a threshold coating percentage for altering the photoreactivity and subsequent phototoxicity of TiO_2.

Table 2 – LC_{50} of TiO_2 nanoparticles to *Escherichia coli*.

Nanoparticles	Anatase	AHA50	AHA200
LC_{50} (ppm)	278.8	201.9	221.9
R^2	0.9295	0.9078	0.9969
Nanoparticles	Rutile	RHA50	RHA200
LC_{50} (ppm)	6.5	21.6	6.7
R^2	0.8603	0.8535	0.9980

LC_{50}: concentration that causes 50% mortality compared to the control group.

It was reported that co-exposure to TiO_2 nanoparticles and HA under simulated sunlight could significantly increase oxidative stress and subsequent toxicity in developing zebrafish (Bar-Ilan et al., 2012; Yang et al., 2013). Additionally, it was suggested that HA could act as both donor and acceptor of electrons to and from the TiO_2 conduction band (CB), without undergoing mineralization (Cho and Choi, 2002). Therefore, we propose a hypothesis for this particular alteration, as presented in Fig. 6. In this system, HA as a sensitizer is firstly activated by visible light irradiation and subsequently, electrons are injected into the CB of TiO_2. The injected electrons then migrate from the lattice to the surface of TiO_2 where they participate in redox reactions with O_2, leading to the generation of superoxide ($O_2^{\cdot-}$). As an acceptor of electrons, HA also accepts electrons from the solution redox couple, making a looping cycle (Meyer, 1997). In addition, HA also serves as hole scavenger that enhances the production of superoxide (Selli et al., 1999; Ryu and Choi, 2004). It was reported that hydroxyl radicals ($^{\cdot}OH$) could react with HA, leading to the formation of humic acid radicals (Wang et al., 2000; Westerhoff et al., 2007). Thus, the surface coating of HA could alter the light absorption property of TiO_2 nanoparticles. Based on this hypothesis, we can expect that in this study, there will be increased superoxide formation, and decreased of $^{\cdot}OH$. It is true so far, for anatase TiO_2. However, the story is slightly different with rutile. The rutile in our experiment had an extremely small band gap, making it sensitive to visible light. It is noteworthy that only a partial visible spectrum (up to 500 nm, corresponding to a band gap of 2.48 eV) is responsible for the light-induced ROS in TiO_2 nanoparticles (Lipovsky et al., 2012). Thus, the low band gap of rutile may not contribute to ROS production any further below 2.48 eV. The coating of HA essentially blocked the light absorption of rutile, while HA *per se* still could be activated by visible light as a sensitizer and a hole scavenger. It was reported that $O_2^{\cdot-}$ was the dominant ROS in rutile upon visible light illumination (Lipovsky et al., 2012). This fact may cause a decrease in the generation of $^{\cdot}OH$ and $O_2^{\cdot-}$ on rutile. The coating of HA at a certain percentage may achieve a maximum interference with light absorption of TiO_2, resulting in a balance of light activation-blocking. In this study, 0.4%–0.5% HA coating on TiO_2 could greatly increase the

Table 3 – Statistic results of viability test by different surface coating and concentration of two types of TiO_2.

Source	Degree of freedom (DF)	Type I SS (sum of squares)	Mean square	F value	Pr > F
Anatase					
Surface coating	2	465.85	232.93	5.25	0.0160
Concentration	2	2792.07	1396.04	31.46	<0.0001
Surface coating-concentration	4	85.48	21.37	0.48	0.7489
Rutile					
Surface coating	2	2826.74	1413.37	12.59	0.0004
Concentration	2	5380.07	2690.04	23.95	<0.0001
Surface coating-concentration	4	1483.93	370.98	3.30	0.0339

photoactivity of anatase, while largely decreasing that of rutile. This hypothesis was then tested with the following investigations on the production of superoxide and hydroxyl radicals upon light activation.

Upon light excitation, excited HA (HA*) transfers electrons (e^-) into the conduction band (CB) of TiO_2. Meanwhile, e^- also transfer back to oxidized HA (HA_{ox}), making a looping cycle. Subsequently, injected e^- lead to the formation of superoxide ($O_2^{\cdot-}$). Hydroxyl radicals ($^{\cdot}OH$) react with HA, resulting in the generation of humic acid radicals ($HA^{\cdot}$), which further promote the production of $O_2^{\cdot-}$. The production of $O_2^{\cdot-}$ and $^{\cdot}OH$ is affected by the balance of HA-photosensitization-light-blocking on the surface of TiO_2 nanoparticles.

2.3. Measurement of reactive oxygen species

ROS is regarded as the critical factor in causing nanotoxicity by disturbing physiological redox-regulated functions, resulting in cellular damage, and death (Fu et al., 2014; He et al., 2014b). In this study, we first measured the generation of hydroxyl radicals. As we expected, rutile generated much more $^{\cdot}OH$ than anatase at the same concentration (Fig. 7). It is also noted that the generation of $^{\cdot}OH$ by RHA50 and RHA200 decreased by 43% and 4% compare to uncoated rutile at 10 ppm ($p < 0.05$), respectively. Similarly, the generation of $^{\bullet}OH$ by AHA50 and AHA200 was 30% and 27% lower than that of uncoated anatse at 10 ppm ($p < 0.05$), respectively. The results disagree with the LC_{50} values reported in Table 2, but support our hypothesis.

The production of $O_2^{\cdot-}$ was then measured for further elaboration. As shown in Fig. 8, it was found that the generation of $O_2^{\cdot-}$ by RHA50 and RHA200 decreased slightly, by 2.9% and 0.2%, respectively, compared to uncoated rutile at 10 ppm. Opposite to rutile, there was an increase in the $O_2^{\cdot-}$ formation by AHA50 and AHA200 by 2.6% and 1.5%, respectively, compared to uncoated anatase at 10 ppm. Although the change in the percentage (%) value was slight, the statistical difference was significant for both anatase and rutile ($p < 0.05$). This also explicitly agrees with our hypothesis.

It is also noteworthy that different pathways of cell death induced by TiO_2 nanoparticles may also be attributable to our experimental results. Braydich-Stolle et al. (2009) reported that anatase TiO_2 nanoparticles induced cell necrosis, while the rutile TiO_2 nanoparticles initiated apoptosis through formation of ROS. Our data indicate that the generation of $O_2^{\cdot-}$ by uncoated rutile was 4.9% more than that of uncoated anatase at 10 ppm ($p < 0.05$). Similarly, rutile induced more $^{\cdot}OH$ than anatase at 10 ppm by 3.5% ($p < 0.05$). Additionally, since rutile generated much lower $^{\cdot}OH$ but much higher $O_2^{\cdot-}$ at the LC_{50} level than did anatase, we can further conclude that $O_2^{\cdot-}$ was the main ROS responsible for the higher toxicity of rutile upon SSL irradiation.

2.4. TEM analysis of nanoparticles—E. coli interaction

The direct contact between nanoparticles and bacteria has been recognized as an important mechanism in causing

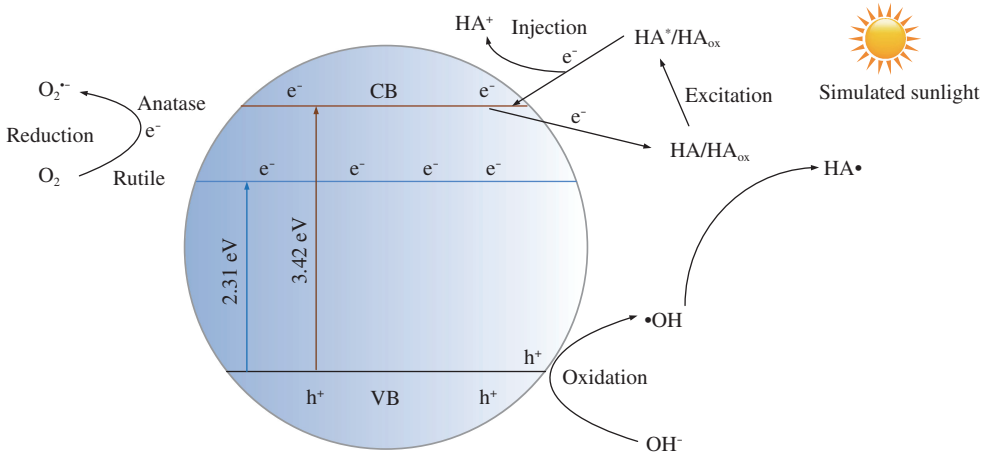

Fig. 6 – Simulated sunlight-induced HA sensitization and hole scavenging on TiO_2. HA^*: excited HA; HA_{ox}: oxidized HA; $HA^{\cdot}$: HA radicals; CB: conduction band; VB: valence band; HA^+: ionized humic acid; HA: humic acid.

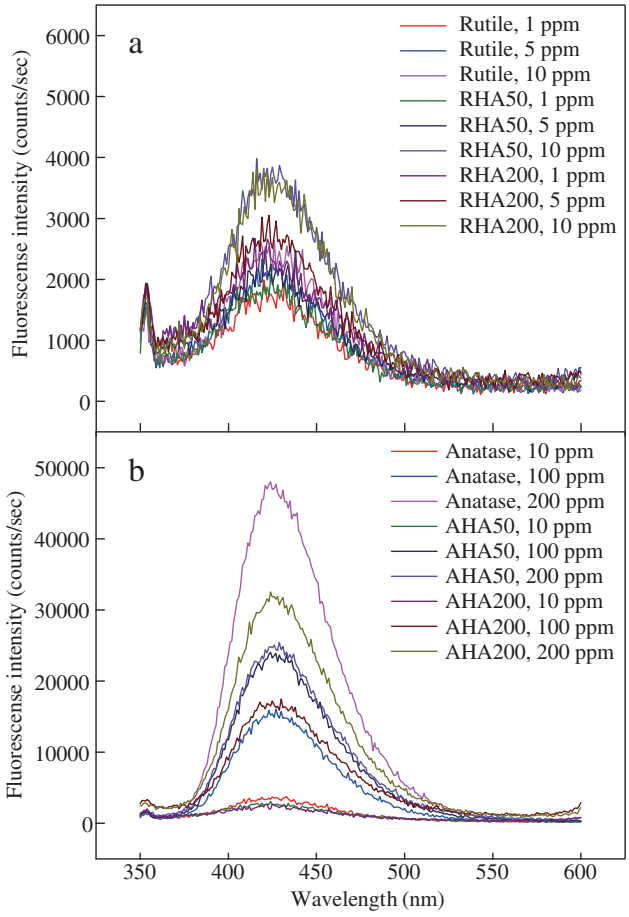

Fig. 7 – Hydroxyl radicals (·OH) generated by (a) rutile and (b) anatase TiO_2 nanoparticles.

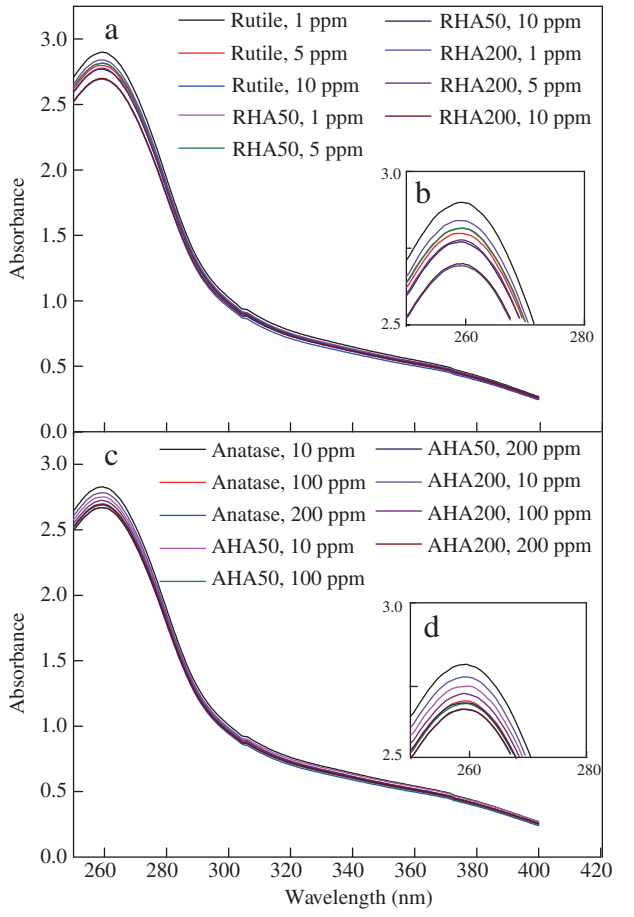

Fig. 8 – Superoxide ($O_2^{\cdot-}$) generated by (a) rutile and (c) anatase TiO_2 nanoparticles. Inserts (b) and (d) are enlargements of absorbance peak portion of (a) and (c), respectively.

cellular toxicity (Jiang et al., 2009). TEM micrographs of nanoparticles—*E. coli* interactions are shown in Fig. 9. The attachment of nanoparticles onto the surface of *E. coli* indicated that there were no preferred sites or arrangements. We did not observe nanoparticles forming any coating on the whole bacterial cells. Intriguingly, all HA coated nanoparticles, including both anatase and rutile, were more likely to attach to bacterial cells, though aggregates were also formed. Unlike uncoated TiO_2, the ones coated with HA were rarely found in other areas except the bacterial surface. Although the number of nanoparticles attached to the bacterial surface is hard to quantify, we noticed that there were more rutile attached to the surface of *E. coli*. This fact may also contribute to the higher toxicity of rutile nanoparticles.

In addition, we also investigated the attachment of TiO_2 nanoparticles onto bacteria in the presence of free HA (Fig. S9). It is clear that TiO_2 nanoparticles randomly scattered all over the grid, in the meantime, attached onto bacterial surface, suggesting that free HA didn't enhance the attachment of nanoparticles as coated HA did. Furthermore, in our previous publication we reported that TiO_2 could pass through cell walls and penetrate the cell membrane, finally entering into the bacterial cell (Pathakoti et al., 2013) and zebrafish cells (He et al., 2014a). We also observed similar results in this study, but no significant difference between anatase and rutile. However, the damage caused by oxidative stress is not solely dependent upon cellular uptake (Heinlaan et al., 2008). Thus, the gathering and attachment of nanoparticles surrounding bacterial surfaces *per se*, may be powerful enough to produce ROS and induce oxidative stress, leading to cellular damage and destruction upon light irradiation.

3. Conclusion

In summary, while both types of the studied TiO_2 nanoparticles were non-toxic in the absences of light, rutile was more toxic to *E. coli* than anatase under SSL. Data suggested that the extreme low band gap of rutile might contribute to its higher SSL-induced activity and toxicity. Humic acid (HA) coating substantially altered the photoactivity and phototoxicity of both anatase and rutile TiO_2 nanoparticles. Clearly, surface-bound HA increased the toxicity of anatase but decreased that of rutile, and exhibited the highest impact at coating percentage of 0.4–0.5%. Analysis results of reactive oxygen species (ROS) implied that superoxide ($O_2^{\cdot-}$) was the main ROS that accounted for higher toxicity of rutile in this study. With HA coating, a pronounced decrease of hydroxyl radicals

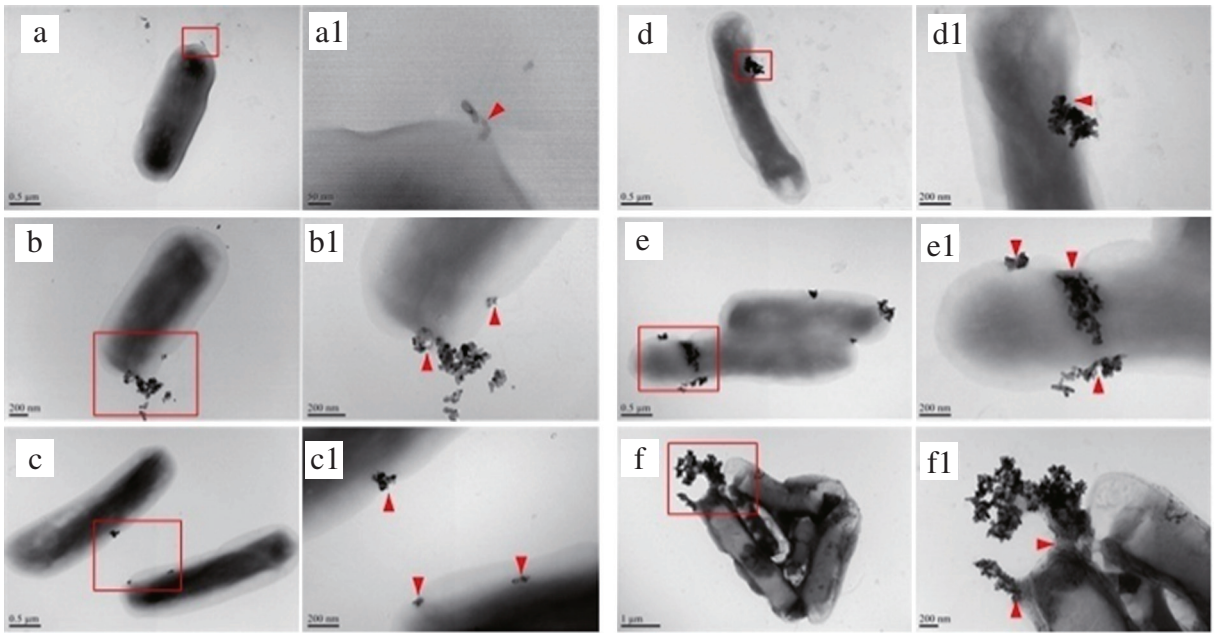

Fig. 9 – Typical TEM micrographs of nanoparticles—*E. coli* interaction. (a–c) Anatase, AHA50, AHA200, magnification at 40,000×, 60,000×, 40,000×, respectively; (d–f) rutile, RHA50, RHA200, magnification at 40,000×, 40,000×, 25,000×, respectively. (a1–c1) and (d1–f1) were enlarged micrographs of the rectangular region in (a–c) and (d–f), magnification at 100,000×, 120,000×, 100,000×, 100,000×, 100,000×, 60,000×, respectively. Red arrow heads indicate where nanoparticles were attached onto *E. coli*.

($^{\cdot}OH$) and O_2^{-} in rutile, a decrease of $^{\cdot}OH$ in anatase and an increase of O_2^{-} in anatase were observed. Finally, TEM analysis revealed the attachment and invasion of nanoparticles into *E. coli*, with a more profound invasion by rutile. In conclusion, from the results of the present study, it is clear that the photocatalytic behavior and toxicological profile of rutile differ from that of anatase TiO_2 nanoparticles (~30 nm) under SSL irradiation. Studies on nano-bio-eco interactions are urgently needed, with emphases on physicochemical properties of TiO_2 nanoparticles and their interactions with DOM and aquatic biota.

Acknowledgments

The study is supported in part by the NSF-REU program (National Science Foundation-Research Experiences for Undergraduates, No. #CHE-1156111) and the NSF-CREST program (National Science Foundation-Centers of Research Excellence in Science and Technology, No. #HRD-0833178). We sincerely thank the technical support from Mississippi State Chemical Laboratory, Mississippi State University for TOC analysis, and School of Polymers and High Performance Materials, the University of Southern Mississippi for SEM, EDX, and XRD characterization.

Appendix A. Supplementary data

Supplementary data to this article can be found online at http://dx.doi.org/10.1016/j.jes.2015.05.028.

REFERENCES

Bar-Ilan, O., Louis, K.M., Yang, S.P., Pedersen, J.A., Hamers, R.J., Peterson, R.E., et al., 2012. Titanium dioxide nanoparticles produce phototoxicity in the developing zebrafish. Nanotoxicology 6 (6), 670–679.

Boxall, A.B., Tiede, K., Chaudhry, Q., 2007. Engineered nanomaterials in soils and water: how do they behave and could they pose a risk to human health? Nanomedicine 2 (6), 919–927.

Braydich-Stolle, L.K., Schaeublin, N.M., Murdock, R.C., Jiang, J., Biswas, P., Schlager, J.J., et al., 2009. Crystal structure mediates mode of cell death in TiO_2 nanotoxicity. J. Nanoparticle Res. 11 (6), 1361–1374.

Chen, X.B., Mao, S.S., 2007. Titanium dioxide nanomaterials: synthesis, properties, modifications, and applications. Chem. Rev. 107 (7), 2891–2959.

Chen, X.D., Wang, Z., Liao, Z.F., Mai, Y.L., Zhang, M.Q., 2007. Roles of anatase and rutile TiO_2 nanoparticles in photooxidation of polyurethane. Polym. Test. 26 (2), 202–208.

Chen, Q.Q., Yin, D.Q., Zhu, S.J., Hu, X.L., 2012. Adsorption of cadmium (II) on humic acid coated titanium dioxide. J. Colloid Interface Sci. 367 (1), 241–248.

Cho, Y., Choi, W., 2002. Visible light-induced reactions of humic acids on TiO_2. J. Photochem. Photobiol. A 148 (1-3), 129–135.

Cook, S.M., Aker, W.G., Rasulev, B.F., Hwang, H.-M., Leszczynski, J., Jenkins, J.J., et al., 2010. Choosing safe dispersing media for C60 fullerenes by using cytotoxicity tests on the bacterium *Escherichia coli*. J. Hazard. Mater. 176 (1-3), 367–373.

De Angelis, F., Fantacci, S., Selloni, A., Nazeeruddin, M.K., Grätzel, M., 2007. Time-dependent density functional theory investigations on the excited states of Ru (II)-dye-sensitized TiO_2 nanoparticles: the role of sensitizer protonation. J. Am. Chem. Soc. 129 (46), 14156–14157.

Fu, P.P., Xia, Q.S., Hwang, H.M., Ray, P.C., Yu, H.T., 2014. Mechanisms of nanotoxicity: generation of reactive oxygen species. J. Food Drug Anal. 22 (1), 64–75.

Goto, H., Hanada, Y., Ohno, T., Matsumura, M., 2004. Quantitative analysis of superoxide ion and hydrogen peroxide produced from molecular oxygen on photoirradiated TiO_2 particles. J. Catal. 225 (1), 223–229.

Guichard, Y., Schmit, J., Darne, C., Gaté, L., Goutet, M., Rousset, D., et al., 2012. Cytotoxicity and genotoxicity of nanosized and microsized titanium dioxide and iron oxide particles in Syrian hamster embryo cells. Ann. Occup. Hyg. 56 (5), 631–644.

He, X., Aker, W.G., Leszczynski, J., Hwang, H.M., 2014a. Using a holistic approach to assess the impact of engineered nanomaterials inducing toxicity in aquatic systems. J. Food Drug Anal. 22 (1), 128–146.

He, X.J., Aker, W.G., Hwang, H.M., 2014b. An *in vivo* study on the photo-enhanced toxicities of S-doped TiO_2 nanoparticles to zebrafish embryos (*Danio rerio*) in terms of malformation, mortality, rheotaxis dysfunction, and DNA damage. Nanotoxicology 8 (S1), 185–195.

Heinlaan, M., Ivask, A., Blinova, I., Dubourguier, H.C., Kahru, A., 2008. Toxicity of nanosized and bulk ZnO, CuO, TiO_2 to bacteria *Vibrio fischeri*, crustaceans *Daphnia magna*, *Thamnocephalus platyurus*. Chemosphere 71 (7), 1308–1316.

Ishibashi, K.-I., Fujishima, A., Watanabe, T., Hashimoto, K., 2000. Quantum yields of active oxidative species formed on TiO_2 photocatalyst. J. Photochem. Photobiol. A 134 (1-2), 139–142.

Jiang, W., Mashayekhi, H., Xing, B.S., 2009. Bacterial toxicity comparison between nano-and micro-scaled oxide particles. Environ. Pollut. 157 (5), 1619–1625.

Kakinoki, K., Yamane, K., Teraoka, R., Otsuka, M., Matsuda, Y., 2004. Effect of relative humidity on the photocatalytic activity of titanium dioxide and photostability of famotidine. J. Pharm. Sci. 93 (3), 582–589.

Kavei, G., Nakaruk, A., Sorrell, C.C., 2011. Equilibrium state of anatase to rutile transformation for titanium dioxide film prepared by ultrasonic spray pyrolysis technique. Mater. Sci. Appl. 2 (6), 700–705.

Kwon, S., Fan, M., Cooper, A.T., Yang, H., 2008. Photocatalytic applications of micro-and nano-TiO2 in environmental engineering. Crit. Rev. Environ. Sci. Technol. 38 (3), 197–226.

Lin, D.H., Ji, J., Long, Z.F., Yang, K., Wu, F.C., 2012. The influence of dissolved and surface-bound humic acid on the toxicity of TiO_2 nanoparticles to Chlorella sp. Water Res. 46 (14), 4477–4487.

Lipovsky, A., levitski, L., Tzitrinovich, Z., Gedanken, A., Lubart, R., 2012. The different behavior of rutile and anatase nanoparticles in forming oxy radicals upon illumination with visible light: An EPR study. Photochem. Photobiol. 88 (1), 14–20.

Luttrell, T., Halpegamage, S., Tao, J., Kramer, A., Sutter, E., Batzill, M., 2014. Why is anatase a better photocatalyst than rutile?— Model studies on epitaxial TiO_2 films. Sci. Rep. 4 (4043), 1–8.

Meyer, G.J., 1997. Efficient light-to-electrical energy conversion: nanocrystalline TiO_2 films modified with inorganic sensitizers. J. Chem. Educ. 76 (6), 652–656.

Numano, T., Xu, J., Futakuchi, M., Fukamachi, K., Alexander, D.B., Furukawa, F., et al., 2014. Comparative study of toxic effects of anatase and rutile type nanosized titanium dioxide particles *in vivo* and *in vitro*. Asian Pac. J. Cancer Prev. 15 (2), 929–935.

Pathakoti, K., Morrow, S., Han, C., Pelaez, M., He, X., Dionysiou, D.D., et al., 2013. Photo-inactivation of *Escherichia coli* by sulfur, nitrogen-fluorine-codoped TiO_2 nanoparticles under solar simulated light, visible light irradiation. Environ. Sci. Technol. 47 (17), 9988–9996.

Persson, P., Bergström, R., Lunell, S., 2000. Quantum chemical study of photoinjection processes in dye-sensitized TiO_2 nanoparticles. J. Phys. Chem. B 104 (44), 10348–10351.

Ryu, J., Choi, W., 2004. Effects of TiO_2 surface modifications on photocatalytic oxidation of arsenite: the role of superoxides. Environ. Sci. Technol. 38 (10), 2928–2933.

Sayes, C.M., Wahi, R., Kurian, P.A., Liu, Y., West, J.L., Ausman, K.D., et al., 2006. Correlating nanoscale titania structure with toxicity: a cytotoxicity and inflammatory response study with human dermal fibroblasts and human lung epithelial cells. Toxicol. Sci. 92 (1), 174–185.

Selli, E., Baglio, D., Montanarella, L., Bidoglio, G., 1999. Role of humic acids in the TiO_2-photocatalyzed degradation of tetrachloroethene in water. Water Res. 33 (8), 1827–1836.

Sharma, V.K., 2009. Aggregation and toxicity of titanium dioxide nanoparticles in aquatic environment— a review. J. Environ. Sci. Health A 44 (14), 1485–1495.

Tayade, R.J., Surolia, P.K., Kulkarni, R.G., Jasra, R.V., 2007. Photocatalytic degradation of dyes and organic contaminants in water using nanocrystalline anatase and rutile TiO_2. Sci. Technol. Adv. Mater. 8 (6), 455–462.

Wang, G.-S., Hsieh, S.-T., Hong, C.-S., 2000. Destruction of humic acid in water by UV light-catalyzed oxidation with hydrogen peroxide. Water Res. 34 (15), 3882–3887.

Warheit, D.B., 2008. How meaningful are the results of nanotoxicity studies in the absence of adequate material characterization? Toxicol. Science 101 (2), 183–185.

Westerhoff, P., Mezyk, S.P., Cooper, W.J., Minakata, D., 2007. Electron pulse radiolysis determination of hydroxyl radical rate constants with Suwannee River fulvic acid and other dissolved organic matter isolates. Environ. Sci. Technol. 41 (13), 4640–4646.

Yang, K., Xing, B.S., 2009. Sorption of phenanthrene by humic acid-coated nanosized TiO_2, ZnO. Environ. Sci. Technol. 43 (6), 1845–1851.

Yang, S.P., Bar-Ilan, O., Peterson, R.E., Heideman, W., Hamers, R.J., Pedersen, J.A., 2013. Influence of humic acid on titanium dioxide nanoparticle toxicity to developing zebrafish. Environ. Sci. Technol. 47 (9), 4718–4725.

Yu, J.G., Dai, G.P., Huang, B.B., 2009. Fabrication and characterization of visible-light-driven plasmonic photocatalyst Ag/AgCl/TiO_2 nanotube arrays. J. Phys. Chem. C 113 (37), 16394–16401.